https://doi.org/10.5194/angeo-2023-2
Preprint. Discussion started: 24 January 2023

Annales Geophysicae Discussions
Open Access
EGU

Potential mapping method for the steady-state magnetosheath model

Yasuhito Narita[1], Simon Toepfer[2], and Daniel Schmid[1]

[1]Space Research Institute, Austrian Academy of Sciences, Schmiedlstr. 6, 8042 Graz, Austria
[2]Institut für Theoretische Physik, Technische Universität Braunschweig, Mendelssohnstr. 3, 38106 Braunschweig, Germany

Correspondence: Y. Narita (yasuhito.narita@oeaw.ac.at)

Abstract. We present the potential mapping method which is a model of steady-state flow velocity and magnetic field in the empirical magnetosheath domain. The method makes use of a coordinate transformation from the empirical magnetosheath domain into the parabolic magnetosheath domain, and evaluate a set of the shell variable and the connector variable to utilize the solution of Laplace equation obtained for the parabolic magnetosheath domain. Our model uses two invariants of transformation: the zenith angle in the magnetosheath and the ratio of the distance to the magnetopause to the thickness of magnetosheath along the magnetopause-normal direction. The plasma flow and magnetic field can be determined as a function of the upstream condition (flow velocity or magnetic field) in a wider range of zenith angle. The potential mapping method is computationally inexpensive by using the analytic expression as much as possible, is applicable to the planetary magnetosheath domains.

1 Modeling the steady-state magnetosheath

Steady-state plasma flow and magnetic field can be regarded as a realization of potential field in the planetary magnetosheath region when the vorticity and the electric current are treated as ignored. In such a case, the potential is obtained by solving the Laplace equation, which was elegantly and analytically solved by Kobel and Flückiger (1994) in a parabolic shape of magnetosheath (hereafter KF). The KF potential was further extended to the stream function in the magnetosheath by Guicking et al. (2012).

The KF solution made a series of breakthroughs in the magnetosheath research. One of the most successful applications is the ability to track the plasma parcel along the streamline in the modeled magnetosheath. The tracking method was extensively used to observationally study the mirror mode growth (e.g., Tatrallyay et al., 2002; Génot et al., 2011) and the streamwise turbulence evolution in the magnetosheath (Guicking et al., 2012). Predictive models of plasma flow and magnetic field serve as a useful tool when combined with the numerical simulation or the observational data.

The KF potential is obtained on the assumption that the planetary bow shock and magnetopause have a parabolic shape sharing the same focal point. Empirical models of the bow shock and magnetopause (fitted to the spacecraft data), on the other hand, are not necessarily parabolically or co-focally shaped. For example, the empirical Earth bow shock model by Farris et al. (1991) and Cairns et al. (1995) has a parabolic shape but the focal point differs from that of the KF solution; the empirical magnetopause model by Shue et al. (1997) applies a power-law scaling to the parabolic shape such that the magnetic field lines appear stretched in the tail region. The gap between the KF parabolic magnetosheath and the empirical magnetosheath needs to be filled when applying the KF potential in the empirical magnetosheath.

https://doi.org/10.5194/angeo-2023-2
Preprint. Discussion started: 24 January 2023

Annales Geophysicae Discussions
Open Access
EGU

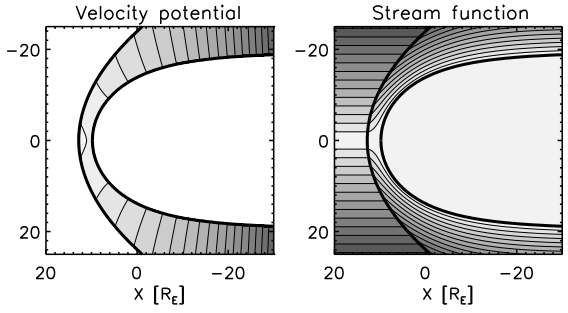

Figure 1. Velocity potential (left panel) and stream function (right panel) in the empirical magnetosheath domain obtained by mapping onto the shell variable v and the connector variable u.

Naively speaking, one wishes to find a conformal mapping from the KF parabolic magnetosheath onto an arbitrary shape of empirical magnetosheath such as the analytic extension of magnetopause shape (Narita et al., 2023). However, it turns out that no general mathematical algorithm is known so far to obtain the conformal mapping when the spatial domain is not properly bounded. The problem lies in the fact that the magnetosheath region is bounded only by two sides, i.e., the standing shock and the magnetopause in the radial direction to the planet, but not bounded along the flow in the tail region. The algorithms of numerical conformal mapping are so far proposed for spatially bounded domains (Papamichael and Whiteman, 1973; Chakravarthy and Anderson, 1979; Fornberg, 1980; Karageorghis et al., 1996) or domains with a closed shape of internal boundaries (Wei et al., 2014).

A non-conformal yet practical mapping to utilize the KF potential is the radial mapping proposed by Soucek and Escoubet (2012). While the radial mapping can reasonably (i.e., with a relatively high accuracy) transform the KF potential into the empirical magnetosheath domain on the dayside, the mapping quality becomes gradually degraded on the tail side due to the conversion effect of the shell shape. In this paper, we construct a novel mapping method (which we call the potential mapping method) as an improved version of the radial mapping. Our method can compute both the plasma flow and the magnetic field in the empirical magnetosheath domain by evaluating the shell variable v and the connector variable u that are used in the KF potential and the stream function. The flow velocity is computed either via the velocity potential as demonstrated in Fig. 1 left panel or via the stream function as demonstrated in Fig. 1 right panel; and the magnetic field is computed via the scalar magnetic potential (Fig. 2). We present the method to determine the KF potential and the stream function in the empirical magnetosheath domain.

Our method is advantageous in that any harmonic functions (solutions of the Laplace equation) can be mapped to any magnetosheath shape. The Kobel-Flückiger potential and the Guicking stream function are examples of the harmonic functions. The Laplace equation in the magnetosheath can be exactly and analytically integrated in the parabolic coordinate system; yet, in reality, the empirical magnetosheath is not parabolic. Our work fills the gap between the parabolic magnetosheath model and the empirical magnetosheath model. We report here that there is a numerical method to find the v and u values reasonably

https://doi.org/10.5194/angeo-2023-2
Preprint. Discussion started: 24 January 2023

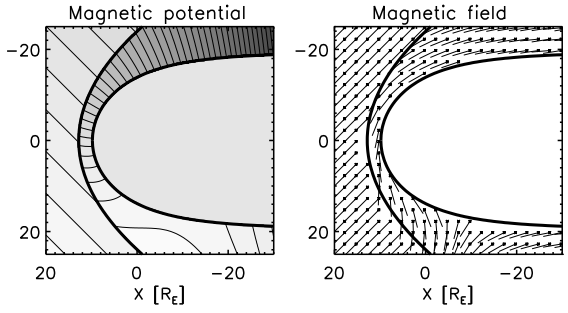

Figure 2. Magnetic potential for the upstream magnetic field with an angle of 135 degree to the x axis (45 degree to the upstream flow direction, (left panel) and sampled magnetic field vectors obtained by the negative gradient of the magnetic potential (right panel).

in an arbitrary magnetosheath shape. We chose a shifted parabolic shape of the bow shock and an empirical shape of the magnetopause. But the algorithm is so general that one can apply the method to other shapes of the shock and magnetopause.

Our study is motivated by the radial mapping method introduced by Soucek and Escoubet (2012). While the radial mapping is nearly boundary-fitted on the dayside, the orthogonality of mapping degrades in the flank to tail region. In our approach, we implement a magnetopause-fitted mapping by retaining two invariants: one is the zenith angle in the magnetosheath to the nearest magnetopause position, and the other is the relative distance from the magnetopause to the bow shock along the magnetopause-normal direction. By doing so, the flow velocity and the magnetic field can be computed in a wider range of zenith angles up to the flank and tail region of magnetosheath. Thus, the present study enables us to generalize the existing models of the flow velocity (e.g., Soucek and Escoubet, 2012; Schmid et al., 2021) and the magnetic field (e.g., Kobel and Flückiger, 1994) within the magnetosheath for more realistic conditions (i.e., magnetopause and bow shock shapes). This mapping method also opens the door to a novel tool development to estimate the interplanetary magnetic field directly from the magnetic field data in the sheath region (Toepfer et al., 2022).

2 Potential field in the magnetosheath

In the frame of potential theory, the flow velocity is $\boldsymbol{U}$ is obtained from the velocity potential $\Phi^{(\mathrm{vel})}$ or from the stream function Ψ as

$$\boldsymbol{U} = -\nabla\Phi^{(\mathrm{vel})} = -\nabla \times (\Psi \boldsymbol{e}_\phi)\,. \tag{1}$$

The symbol $\boldsymbol{e}_\phi$ is the unit vector in the azimuthal directions around the symmetry axis (Sun-to-planet direction). Kobel and Flückiger (1994) and Guicking et al. (2012) obtained the analytic expression of the velocity potential $\Phi^{(\mathrm{vel})}$ using the shell variable v (iso-contour lines enveloping the magnetosphere) and the connector variable u (iso-contour lines connecting from

https://doi.org/10.5194/angeo-2023-2
Preprint. Discussion started: 24 January 2023

Annales Geophysicae Discussions
Open Access
EGU

the bow shock to the magnetopause).

$$\Phi^{(\mathrm{vel})} = -U_x \left(\frac{v_{\mathrm{mp}}^2 v_{\mathrm{bs}}^2}{v_{\mathrm{bs}}^2 - v_{\mathrm{mp}}^2} \right) \left(\frac{u^2 - v^2}{2 v_{\mathrm{bs}}^2} + \ln v \right) - \frac{1}{2} U_x \left(u^2 - v^2 \right) + \Phi_0^{(\mathrm{vel})}, \tag{2}$$

where U_x is the upstream flow velocity, v_{mp} the shell variable at the magnetopause, v_{bs} the shell variable at the bow shock, v the shell variable, u the connector variable, and $\Phi_0^{(\mathrm{vel})}$ a free parameter (integration constant) which is set to zero without loss of generality. The shell variables v_{mp} and v_{bs} contain the information on the stand-off distances (R_{mp} and R_{bs}) in the subsolar region, and are defined by Kobel and Flückiger (1994) as

$$v_{\mathrm{mp}} = \sqrt{R_{\mathrm{mp}}} \tag{3}$$

$$v_{\mathrm{bs}} = \sqrt{2R_{\mathrm{bs}} - R_{\mathrm{mp}}}. \tag{4}$$

Guicking et al. (2012) transformed the KF potential and obtained analytically the stream function Ψ as a function of the shell variable and the connector variable:

$$\Psi = -\frac{1}{2} U_x \left(\frac{v_{\mathrm{mp}}^2 v_{\mathrm{bs}}^2}{v_{\mathrm{bs}}^2 - v_{\mathrm{bs}}^2} \right) \frac{u}{v} \left(\frac{v^2}{v_{\mathrm{bs}}^2} - 1 \right) - \frac{1}{2} U_x u v. \tag{5}$$

Hereafter, one may set $U_x = -1$ so that the velocity potential $\Phi^{(\mathrm{vel})}$ is normalized to the upstream velocity.

The magnetic field in the magnetosheath is derived from the potential in the same fashion as the flow velocity, that is,

$$\boldsymbol{B} = -\nabla \Phi^{(\mathrm{mag})}. \tag{6}$$

The magnetic potential is a function of the shell variable v and the connector variable u (Kobel and Flückiger, 1994):

$$\Phi^{(\mathrm{mag})} = -\frac{v_{\mathrm{mp}}^2 v_{\mathrm{bs}}^2}{v_{\mathrm{bs}}^2 - v_{\mathrm{mp}}^2} \times \left[\left(B_y^{(\mathrm{up})} \cos\phi + B_z^{(\mathrm{up})} \sin\phi \right) u \left(\frac{1}{v} + \frac{v}{v_{\mathrm{bs}}^2} \right) + B_x^{(\mathrm{up})} \left(\frac{u^2 - v^2}{2 v_{\mathrm{bs}}^2} + \ln v \right) \right] - B_x^{(\mathrm{up})}(-x) - B_y^{(\mathrm{up})} y - B_z^{(\mathrm{up})} z + \Phi_0^{(\mathrm{mag})}, \tag{7}$$

where $B_x^{(\mathrm{up})}$ is the sunward component of the upstream magnetic field (corresponding to the GSE-X in near-Earth space), and $B_y^{(\mathrm{up})}$ and $B_z^{(\mathrm{up})}$ are two components of the upstream magnetic field perpendicular to the x direction. ϕ is the azimuthal angle of the position around the symmetry axis (the y direction is given by the angle $\phi = 0$). The integration constant is chosen as $\Phi_0^{(\mathrm{mag})} = 0$. The magnetic potential cannot be further transformed into the form of stream function since the magnetic field distribution is essentially three-dimensional in the magnetosheath.

https://doi.org/10.5194/angeo-2023-2
Preprint. Discussion started: 24 January 2023

Annales Geophysicae Discussions
Open Access
EGU

The shell variable v and the connector u play an important role in computing the flow velocity and magnetic field in the magnetosheath. These variables are explicitly evaluated in the style of parabolic coordinates as

$$v = \sqrt{r_0 + (x_\mathrm{k} - x_0)} \tag{8}$$

$$u = \sqrt{r_0 - (x_\mathrm{k} - x_0)}, \tag{9}$$

where r_0 is the distance to the focus at x_0:

$$r_0 = \sqrt{(x_\mathrm{k} - x_0)^2 + y_\mathrm{k}^2 + z_\mathrm{k}^2} \tag{10}$$

and the focus is along the x axis, and is defined as

$$x_0 = \frac{1}{2} R_\mathrm{mp}. \tag{11}$$

x_k, y_k, and z_k are the Cartesian representation of the KF magnetosheath model (i.e., with the pre-fixed bow shock and magnetopause shapes) obtained by projecting the position vector onto the unit vectors $\boldsymbol{e}_x$, $\boldsymbol{e}_y$, and $\boldsymbol{e}_z$:

$$x_\mathrm{k} = \boldsymbol{r}^{(\mathrm{k})} \cdot \boldsymbol{e}_x \tag{12}$$

$$y_\mathrm{k} = \boldsymbol{r}^{(\mathrm{k})} \cdot \boldsymbol{e}_y \tag{13}$$

$$z_\mathrm{k} = \boldsymbol{r}^{(\mathrm{k})} \cdot \boldsymbol{e}_z. \tag{14}$$

To complete the variable set for computing the potentials and the stream function, the azimuthal angle ϕ is introduced as

$$\phi = \mathrm{atan}(z_\mathrm{k}/y_\mathrm{k}). \tag{15}$$

Our task is to find the shell variable v and the connector variable u in the empirical magnetosheath by finding a suitable mapping of the position vector from the empirical magnetosheath (denoted by $\boldsymbol{r}$) onto the KF parabolic system (denoted by $\boldsymbol{r}^{(\mathrm{k})}$). The evaluated v and u are then readily used to obtain the scalar potentials and the stream function. The flow velocity and the magnetic field in the empirical magnetosheath are obtained by computing the gradient of the respective potential. Figure 3 visualizes the iso-contours of the shell variable v and the connector variable u in the KF parabolic system (left panel) and the empirical magnetosheath (right panel). The shell variable v is characterized by the lines with the curvature center on the right side in the panel, and contains the parabolic bow shock (at $v = v_\mathrm{bs}$) and magnetopause (at $v = v_\mathrm{mp}$) marked by thick lines. The connector variable u has the curvature center on the left side in the panel, and the iso-contour lines are orthogonal to the bow shock and magnetopause. Our mapping procedure evaluates the scalar potential in the empirical magnetosheath by transforming the coordinates from the empirical magnetosheath into the KF magnetosheath model as $(x, y, z) \rightarrow (x_\mathrm{k}, y_\mathrm{k}, z_\mathrm{k})$, and evaluating the key variables v (the shell variable) and u (the connector variable) in the KF magmetosheath model as $(x_\mathrm{k}, y_\mathrm{k}, z_\mathrm{k}) \rightarrow (u, v, \phi)$.

https://doi.org/10.5194/angeo-2023-2
Preprint. Discussion started: 24 January 2023

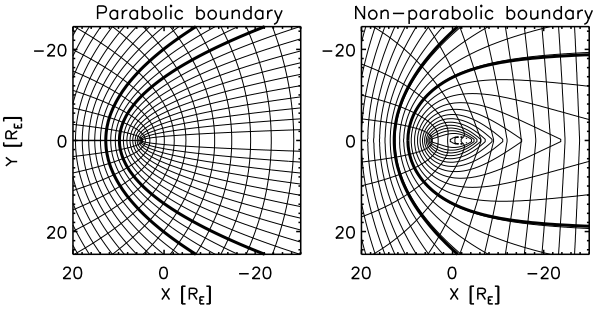

Figure 3. Iso-contour lines with $u = \mathrm{const.}$ (center of curvature on the left side) and that with $v = \mathrm{const.}$ (center of curvature on the right side) in the KF magnetosheath model (left panel) and the empirical magnetosheath model (right panel). The bow shock stand-off distance is 12.8 Earth radii and the magnetopause stand-off distance is 9.8 Earth radii.

3 Mapping procedure

3.1 Overview of the mapping

The mapping is performed, conceptually speaking, in two transformations to utilize the KF potential and the Guicking stream function (originally developed for the parabolic magnetosheath domain) for the empirical magnetosheath (which is not parabolic). In the first transformation, the position vector is mapped from the empirical magnetosheath $\boldsymbol{r}$ onto the KF system $\boldsymbol{r}_{\mathrm{k}}$. This is achieved on the assumption that the distance from the position in the magnetosheath to the magnetopause along the magnetopause-normal direction is the same when normalized to the magnetosheath thickness (the distance from the bow shock to the magnetopause along the magnetopause-normal direction) and also that the azimuthal angle ϕ is the same between the empirical magnetosheath and the KF system. The first transformation is divided into computing the planet-to-bow shock distance (step 1), the planet-to-magnetopause distance (step 2), magnetosheath-to-magnetopause distance (step 3), the thickness of the empirical magnetosheath (step 4), the thickness of the KF magnetosheath (step 5), and the mapping of the position vector (step 6). In the second transformation, the mapped position vector is used to compute the shell variable v and the connector variable u (step 7) and to obtain the potentials and the stream function in the empirical magnetosheath using Eqs. (2), (5), and (7) (step 8). Here again, the azimuthal angle ϕ is treated as invariant. Figure 4 illustrates the mapping procedure and graphically explains the variables that need to be determined to perform the mapping such as the zenith angle of the nearest magnetopause θ_{mp}, the radial distance to the bow shock and magnetopause along the magnetosheath-normal direction (r_{bs} and r_{mp}, respectively), the distance from the magnetosheath to the magnetopause α_{emp}, the magnetopause thickness $\alpha_{\mathrm{emp}}^{(\mathrm{bs})}$. The position vector $\boldsymbol{r}$ and the bow shock and magnetopause stand-off distances (R_{bs} and R_{mp}) are the input parameters in the model.

https://doi.org/10.5194/angeo-2023-2
Preprint. Discussion started: 24 January 2023

Annales Geophysicae Discussions
Open Access
EGU

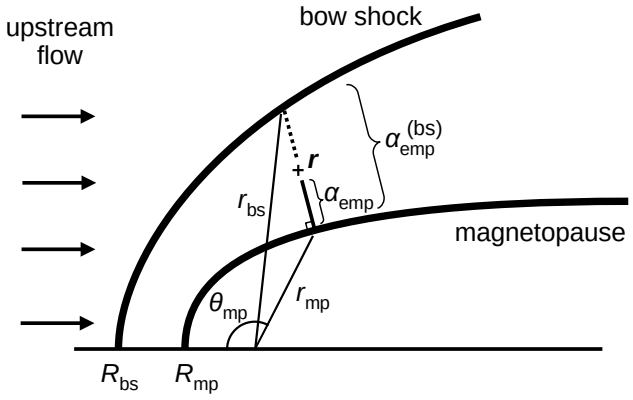

Figure 4. Graphical representation of the variables computed in the step 1 to 4 of the potential mapping method: the zenith angle of the nearest magnetopause $\theta_{\rm mp}$, the radial distance to the bow shock and magnetopause along the magnetosheath-normal direction ($r_{\rm bs}$ and $r_{\rm mp}$, respectively), the distance from the magnetosheath to the magnetopause $\alpha_{\rm emp}$, the magnetopause thickness $\alpha_{\rm emp}^{\rm (bs)}$. The position vector $\boldsymbol{r}$ and the bow shock and magnetopause stand-off distances ($R_{\rm bs}$ and $R_{\rm mp}$) are the input parameters in the model.

3.2 Step 1: Computing the planet-to-bow shock distance

We begin with a position vector in the empirical magnetosheath domain, and express the position vector as $\boldsymbol{r} = x\boldsymbol{e}_x + y\boldsymbol{e}_y + z\boldsymbol{e}_z$. Hereafter, we present the mapping procedure in the two-dimensional plane spanning the x and y directions for simplicity, but the computation in three dimensions is straightforward by representing the y component of position vector in the cylindrical fashion as $\rho\cos\phi$ and the z component into $\rho\sin\phi$ using the distance ρ to the x axis. The boundaries (bow shock and magnetopause) are specified by the users and do not need to be parabolic. In this paper, we choose the empirical parabolic bow shock for the outer boundary and the empirical magnetopause as the inner boundary. The empirical bow shock position is expressed in GSE coordinates (the x-axis pointing to the Sun) as (Farris et al., 1991; Cairns et al., 1995)

$$x \;=\; R_{\rm bs} - b_{\rm emp}\, y^2, \tag{16}$$

where $R_{\rm bs}$ is the bow shock stand-off distance and $b_{\rm emp}$ is the empirical flaring parameter.

We express the empirical bow shock in the polar representation using a quadratic equation. The focus is located at the planet. By introducing the zenith angle θ and inserting $x = r_{\rm bs}\cos\theta$ and $y = r_{\rm bs}\sin\theta$ in Eq. 16), we obtain the equation for the radial distance to the empirical bow shock:

$$b_{\rm emp}\, r_{\rm bs}^2 \sin^2\theta + r_{\rm bs}\cos\theta - R_{\rm bs} = 0. \tag{17}$$

https://doi.org/10.5194/angeo-2023-2
Preprint. Discussion started: 24 January 2023


Annales Geophysicae Discussions

Equation (17) can be algebraically solved, and we take the positive value of the solution as

$$r_{\rm bs} = \frac{1}{2b_{\rm emp}\sin^2\theta}\left(-\cos\theta + \sqrt{1-(1-4b_{\rm emp}R_{\rm bs})\sin^2\theta}\right). \tag{18}$$

3.3 Step 2: Computing the planet-to-magnetopause distance

The realistic magnetopause shape significantly differs from the KF system in (1) having the focal point at the planet and (2) exhibiting an asymptotic behavior to a cylindrical shape in the tail region. These features are elegantly incorporated into the empirical magnetopause model by Shue et al. (1997):

$$x^2 + y^2 - \frac{4R_{\rm mp}^4}{4R_{\rm mp}^2 - y^2} = 0, \tag{19}$$

in the Cartesian representation and

$$r_{\rm mp} = R_{\rm mp}\sqrt{\frac{2}{1+\cos\theta}}. \tag{20}$$

in the polar representation. The radial distance to the magnetopause is given conveniently by Eq. (20). The Shue model reproduces the magnetopause stand-off distance $R_{\rm mp}$ in the subsolar direction ($\theta = 0$), the cylindrical distance asymptotes to $2R_{\rm mp}$ in the tail.

3.4 Step 3: Computing the magnetosheath-to-magnetopause distance

We wish to express the position vector along the empirical magnetopause-normal direction such as

$$\boldsymbol{r} = \boldsymbol{r}_{\rm mp} + \alpha_{\rm emp}\,\boldsymbol{e}_{\rm mp}, \tag{21}$$

where $\boldsymbol{r}_{\rm mp}$ is the magnetopause position nearest to the position vector, and $\boldsymbol{e}_{\rm mp}$ is the unit vector in the magnetopause-normal direction. The unit vector points away from the planet and satisfies the condition

$$\boldsymbol{r}_{\rm mp}\cdot\boldsymbol{e}_{\rm mp} > 0 \tag{22}$$

The symbol $\alpha_{\rm emp}$ is the distance to the magnetopause along the magnetopause-normal direction $\boldsymbol{e}_{\rm mp}$ in the empirical magnetosheath.

The nearest magnetopause position is obtained by searching for the zenith angle $\theta_{\rm mp}$ for the minimum distance from the sample position to the magnetopause. The distance D is defined as

$$D = \sqrt{(r_x - r_{\rm mp}\cos\theta_{\rm mp})^2 + (r_y - r_{\rm mp}\sin\theta_{\rm mp})^2}. \tag{23}$$

https://doi.org/10.5194/angeo-2023-2
Preprint. Discussion started: 24 January 2023

Annales Geophysicae Discussions
Open Access
EGU

The search for the minimum distance is implemented in a brute-force fashion as a function of $\mu_{\rm mp} = \cos\theta_{\rm mp}$ in our study. It is worth noting that the variation of D^2 with respect to $\mu_{\rm mp}$ has an analytic expression as

$$\begin{aligned}\frac{\delta(D^2)}{\delta\mu_{\rm mp}} &= \frac{1}{2R_{\rm mp}} - \frac{2}{R_{\rm mp}}\frac{1}{\sqrt{(1+\mu_{\rm mp})/2}} \times \\ &\left[\frac{1}{4}(r_x\mu_{\rm mp} - r_y\sqrt{1-\mu_{\rm mp}^2}) + \right. \\ &\left.\frac{1+\mu_{\rm mp}}{2}\left(r_x + \frac{r_y\mu_{\rm mp}}{1-\mu_{\rm mp}^2}\right)\right] \end{aligned} \tag{24}$$

and one may alternatively search for $\mu_{\rm mp}$ satisfying the condition:

$$\frac{\delta(D^2)}{\delta\mu_{\rm mp}} = 0. \tag{25}$$

Having the nearest magnetopause at a distance of $r_{\rm mp}$ and a zenith angle of $\theta_{\rm mp}$, we are ready to compute the magnetopause-normal direction and the distance $\alpha_{\rm emp}$. To obtain the magnetopause-normal direction, we define the magnetopause shape function $f_{\rm mp}$ as

$$f_{\rm mp} = x^2 + y^2 - \frac{4R_{\rm mp}^4}{4R_{\rm mp}^2 - y^2}, \tag{26}$$

and compute the normal direction by the gradient of $f_{\rm mp}$ as

$$\frac{\partial f_{\rm mp}}{\partial x} = 2x \tag{27}$$

$$\frac{\partial f_{\rm mp}}{\partial y} = 2y\left[1 - \frac{4R_{\rm mp}^4}{(4R_{\rm mp}^2 - y^2)^2}\right]. \tag{28}$$

The magnetopause-normal direction is obtained by normalizing the gradient vector $(\partial_x f_{\rm mp}, \partial_y f_{\rm mp})$ and representing with the basis vectors ($\boldsymbol{e}_x$ and $\boldsymbol{e}_y$) as

$$\begin{aligned}\boldsymbol{e}_{\rm mp} &= \frac{\rm sgn}{\sqrt{(\partial_x f_{\rm mp})^2 + (\partial_y f_{\rm mp})^2}} \times \\ &(\partial_x f_{\rm mp}\,\boldsymbol{e}_{\rm x} + \partial_y f_{\rm mp}\,\boldsymbol{e}_{\rm y}) \end{aligned} \tag{29}$$

evaluated at the magnetopause ($x = r_{\rm mp}\cos\theta_{\rm mp}$ and $y = r_{\rm mp}\sin\theta_{\rm mp}$). The magnetopause-normal vector $\boldsymbol{e}_{\rm mp}$ has a unit length, and the sign (${\rm sgn} = \pm 1$) is chosen such that the normal vector is pointing outward (Eq. 22). The distance $\alpha_{\rm emp}$ to the magnetopause along the normal direction is obtained from Eq. (21) as

$$\alpha_{\rm emp} = \frac{(x - r_{\rm mp}\cos\theta_{\rm mp}) + (y - r_{\rm mp}\sin\theta_{\rm mp})}{\boldsymbol{e}_{\rm mp}\cdot\boldsymbol{e}_x + \boldsymbol{e}_{\rm mp}\cdot\boldsymbol{e}_y} \tag{30}$$

Equation (30) is constructed to be robust against the singular behavior on the dayside ($\boldsymbol{e}_{\rm mp}\cdot\boldsymbol{e}_y = 0$) and in distant tail ($\boldsymbol{e}_{\rm mp}\cdot\boldsymbol{e}_x = 0$).

https://doi.org/10.5194/angeo-2023-2
Preprint. Discussion started: 24 January 2023

Annales Geophysicae Discussions
Open Access
EGU

3.5 Step 4: Computing the thickness of empirical magnetosheath

For our mapping purpose, the distance $\alpha_{\rm emp}$ is normalized to the magnetosheath thickness $\alpha_{\rm emp}^{\rm (bs)}$ such that relative distance $\alpha_{\rm emp}/\alpha_{\rm emp}^{\rm (bs)}$ serves as an invariant of the mapping from the empirical magnetosheath onto the KF magnetosheath. To achieve this, we combine Eq. (16) with Eq. (21), and analytically determine the thickness from the bow shock to the magnetopause in the empirical magnetosheath. That is, the thickness $\alpha_{\rm emp}^{\rm (bs)}$ is obtained by rewriting the bow shock quadratic equation (Eq. 16) for the position vector using the variable $\alpha_{\rm emp}^{\rm (bs)}$ (Eq. 21) extended to the bow shock location. The equation is again quadratic, and the solution is algebraically obtained as:

$$\begin{aligned}\alpha_{\rm emp}^{\rm (bs)} &= \frac{1}{2b_{\rm emp}\, e_{{\rm mp},y}^2} \times \\ &\quad \left[-(e_{{\rm mp},x} + 2b_{\rm emp}\, y_{\rm mp} e_{{\rm mp},y})^2 + d_\alpha\right], \end{aligned} \tag{31}$$

where d_α is an auxiliary variable defined as

$$\begin{aligned} d_\alpha &= [(e_{{\rm mp},x} + 2b_{\rm emp}\, y_{\rm mp}\, e_{{\rm mp},y})^2 - \\ &\quad 4b_{\rm emp}\, e_{{\rm mp},y}^2 \times \\ &\quad (x_{\rm mp} + b_{\rm emp}\, y_{\rm mp}^2 - R_{\rm bs})]^{1/2}. \end{aligned} \tag{32}$$

In the subsolar direction ($y_{\rm mp} = 0$), the thickness is simplified to

$$\alpha_{\rm emp}^{\rm (bs)} = R_{\rm bs} - R_{\rm mp}. \tag{33}$$

3.6 Step 5: Computing the magnetosheath thickness in the KF system

Now we repeat the procedures from the step 1 to 5 for the KF system to determine the magnetosheath thickness in the KF system $\alpha^{\rm (k)}$. We treat the zenith angle $\theta_{\rm mp}$ and the relative distance $\alpha_{\rm emp}/\alpha_{\rm emp}^{\rm (bs)}$ as invariants of the mapping between the empirical magnetosheath and the KF system. The KF bow shock location is given as

$$x = R_{\rm bs} - b_{\rm k} y^2, \tag{34}$$

where the KF bow-shock flaring parameter $b_{\rm k}$ is pre-fixed as (Kobel and Flückiger, 1994)

$$b_{\rm k} = \frac{1}{4R_{\rm bs} - 2R_{\rm mp}}. \tag{35}$$

The radial distance from the planet to the KF bow shock is

$$\begin{aligned} r_{\rm bs}^{\rm (k)} &= \frac{1}{2b_{\rm k}\sin^2\theta} \times \\ &\quad \left(-\cos\theta + \sqrt{1 + (4b_{\rm k}R_{\rm bs} - 1)\sin^2\theta}\right). \end{aligned} \tag{36}$$

The KF magnetopause is defined in Kobel and Flückiger (1994) as

$$x = R_{\rm mp} - \frac{1}{2R_{\rm mp}} y^2. \tag{37}$$

https://doi.org/10.5194/angeo-2023-2
Preprint. Discussion started: 24 January 2023

Annales Geophysicae Discussions

From Eq. (37) the radial distance from the planet to the KF magnetopause is computed as

$$r_{\rm mp}^{\rm (k)} = \frac{R_{\rm mp}}{\sin^2\theta}\left(-\cos\theta+\sqrt{1+\sin^2\theta}\right). \tag{38}$$

To obtain the magnetopause-normal direction in the KF system, we compute the gradient of the magnetopause shape function:

$$f_{\rm mp}^{\rm (k)} = 2 - R_{\rm mp} + \frac{1}{2R_{\rm mp}}y^2. \tag{39}$$

The gradient is analytically given as

$$\frac{\partial f_{\rm mp}^{\rm (k)}}{\partial x} = 1 \tag{40}$$

$$\frac{\partial f_{\rm mp}^{\rm (k)}}{\partial y} = \frac{y}{R_{\rm mp}} \tag{41}$$

The magnetopause-normal direction $\boldsymbol{e}_{\rm mp}^{\rm (k)}$ is then obtained by applying Eqs. (40) and (41) to Eq. (29), which reads as

$$\boldsymbol{e}_{\rm mp}^{\rm (k)} = \frac{\rm sgn}{\sqrt{(\partial_x f_{\rm mp}^{\rm (k)})^2+(\partial_y f_{\rm mp}^{\rm (k)})^2}}\times \left(\partial_x f_{\rm mp}^{\rm (k)})\,\boldsymbol{e}_{\rm x}+\partial_y f_{\rm mp}^{\rm (k)})\,\boldsymbol{e}_{\rm y}\right) \tag{42}$$

The thickness in the KF system $\alpha_{\rm k}^{\rm (bs)}$ is determined by combining the bow shock shape (Eq. 34) with the position vector at the bow shock:

$$\boldsymbol{r}_{\rm bs}^{\rm (k)} = \boldsymbol{r}_{\rm mp}^{\rm (k)} + \alpha_{\rm k}^{\rm (bs)}\boldsymbol{e}_{\rm mp}^{\rm (k)}. \tag{43}$$

Equation (34) becomes again a quadratic equation with respect to the thickness $\alpha_{\rm k}^{\rm (bs)}$, and the solution reads:

$$\alpha_{\rm k}^{\rm (bs)} = \frac{1}{2b_{\rm k}\,e_{{\rm mp},y}^2}\times \left[-(e_{{\rm mp},x}+2b_{\rm k}\,y_{\rm mp}\,e_{{\rm mp},y})+d_\alpha^{\rm (k)}\right] \tag{44}$$

where the auxiliary variable $d_\alpha^{\rm (k)}$ is defined as

$$d_\alpha^{\rm (k)} = [(e_{{\rm mp},x}+2b_{\rm k}\,y_{\rm mp}\,e_{{\rm mp},y})^2 - -4b_{\rm k}\,e_{{\rm mp},y}^2(x_{\rm mp}+b_{\rm k}y_{\rm mp}^2-R_{\rm bs})]^{1/2}. \tag{45}$$

3.7 Step 6: Mapping the position vector onto the KF system

The mapping of the position vector from the empirical magnetosheath onto the KF system is performed by assuming the relative distance (magnetosheath-to-magnetopause distance normalized to the magnetosheath thickness along the magnetopause-normal direction) is the same between the two systems. The distance from the magnetosheath position vector to the magnetopause along the magnetopause-normal direction in the KF system $\alpha_{\rm k}$ is then determined by the relative distance in the empirical magnetosheath $\alpha_{\rm emp}$, the thickness of the empirical magnetosheath $\alpha_{\rm emp}^{\rm bs}$, and magnetosheath thickness in the KF system $\alpha_{\rm k}^{\rm (bs)}$ as

$$\alpha_{\rm k} = \alpha_{\rm emp}\,\alpha_{\rm k}^{\rm (bs)}/\alpha_{\rm emp}^{\rm (bs)}. \tag{46}$$

https://doi.org/10.5194/angeo-2023-2
Preprint. Discussion started: 24 January 2023

Annales Geophysicae Discussions

The mapped position vector is then computed as

$$\boldsymbol{r}^{(\mathrm{k})} = \boldsymbol{r}^{(\mathrm{k})}_{\mathrm{mp}} + \alpha_{\mathrm{k}}\, \boldsymbol{e}^{(\mathrm{k})}_{\mathrm{mp}}, \tag{47}$$

using the nearest magnetopause position $\boldsymbol{r}^{(\mathrm{k})}_{\mathrm{mp}}$ (Eq. 38), the magnetosheath-to-magnetopause distance α_{k} (Eq. 46), and the magnetopause-normal direction $\boldsymbol{e}^{(\mathrm{k})}_{\mathrm{mp}}$ (Eq. 42).

3.8 Step 7: Computing the shell and connector variables

The shell variable v and the connector variable u are computed from the mapped position vector $\boldsymbol{r}^{(\mathrm{k})}$ using Eqs. (8) and (9). respectively. The variables v and u are the same as the parabolic coordinates used in the KF potential with a focus at $x_0 = R_{\mathrm{mp}}/2$. In our algorithm, the focus is explicitly given in Eqs. (8), (9), and (10). The azimuthal angle around the symmetry axis ϕ is treated in the same way as in the KF paper. Figure 3 compares the iso-contours of the shell v and the connector u represented in the KF system (left panel) and the empirical magnetosheath (right panel) for a bow shock stand-off distance of 12.8 R_{E} (Génot et al., 2011), a bow shock flaring of 0.0223 R_{E}^{-1}, (Farris et al., 1991; Cairns et al., 1995), and a magnetopause stand-off distance 9.8 R_{E} (Génot et al., 2011). The shell variable v is characterized by the lines with the curvature center on the right side in the panel, and contains the parabolic bow shock (at $v = v_{\mathrm{bs}}$) and magnetopause (at $v = v_{\mathrm{mp}}$) marked by thick lines. The connector variable u has the curvature center on the left side in the panel, and the iso-contour lines are orthogonal to the bow shock and magnetopause. The mesh pattern in the KF parabolic system (Fig. 3) is symmetric with respect to exchanging between v and u at the focal point $X = R_{\mathrm{mp}}/2$, while the mesh in the empirical magnetosheath is asymmetric between v and u.

3.9 Step 8: Computing the potentials and stream function

The scalar potentials (velocity potential and magnetic potential) and the stream function are obtained from the shell v and the connector u using Eqs. (2), (5), and (7). The velocity potential (normalized to the upstream flow) is displayed in Fig. 1 left panel, and the stream function in right panel. The iso-contours of the velocity potential represent the lines of the same flow velocity. The iso-contours of the stream function represent the streamline in the magnetosheath. The flow is deflected around the nose of magnetopause (the subsolar point) and the streamlines are tangential to the magnetopause.

The magnetic potential and the derived magnetic field are displayed in Fig. 2. The magnetic potential and the magnetic field (the gradient of the potential multiplied by the minus sign) depend on the upstream field. Fig. 2 shows an example with an upstream field angle of 135 degree to the x axis (i.e., 45 degree to the upstream flow direction). The magnetic field is computed using the central difference scheme. Near the boundaries (bow shock or magnetopause), the mesh resolution is enhanced so that the mesh points do not cross the boundary when computing with the central difference scheme. The upstream field is deflected on the positive y side (right panel, lower half plane), and is draping the magnetopause on the negative y side (right panel, upper half plane).

https://doi.org/10.5194/angeo-2023-2
Preprint. Discussion started: 24 January 2023


Annales Geophysicae Discussions Open Access EGU

4 Concluding remark

Our potential mapping method may be regarded as an updated version of the radial mapping method (Soucek and Escoubet, 2012) by retaining the orthogonality near the magnetopause in the flank to tail region and also by computing the field through the potential mapping. Velocity potential, stream function, and magnetic potential are evaluated in the empirical magnetosheath.

The advantages of our methods are as follows.

1. The method makes extensive use of the exact solution of the Laplace equation (the Kobel-Flückiger potential and the Guicking stream function). The plasma flow and magnetic field can be determined semi-analytically in a wider range of zenith angle in the magnetosheath when the solar wind condition and the boundary shapes are given.

2. The method is applicable to an arbitrary shape of magnetosheath domain, opening the door to develop a tool to assist numerical simulations and spacecraft observations of not only the Earth but also the planetary magnetosheath domain.

3. The method is computationally inexpensive. In particular, if the shape of bow shock and magnetopause is analytically given, most of the computational steps in the potential mapping method have an analytic expression.

Naively speaking, as stated in sec. 1, one ideally needs to find a conformal mapping from the KF magnetosheath model onto the empirical magnetosheath. While the conformal mapping is known both for the empirical bow shock and the empirical magnetopause, the conformal mapping of the entire magnetosheath domain still remains a challenge. There are two problems on this. First, the closing boundary (the u-lines) connecting between the bow shock and the magnetopause is not known, and moreover, the uniqueness of finding such a boundary is not guaranteed. Second, the gradients along u are not the same between the empirical bow shock and the empirical magnetopause such that a naive transfinite interpolation ends up with highly non-orthogonal grids in the magnetosheath.

Our method of computing the plasma flow and magnetic field should be compared against the observations and simulations. For example, THEMIS and ARTEMIS spacecraft (Angelopoulos, 2008) and MMS spacecraft (Burch et al., 2016) are providing a huge amount of data on both sides of the bow shock in the equatorial plane; Cluster spacecraft Escoubet et al. (2001) are collecting data in polar orbit; ACE spacecraft data Stone et al. (1998) may be used as an upstream monitor; and Earth flyby data of planetary missions (such as Cassini, BepiColombo) cover the far-distance tail region. In reality, non-axisymmetric structure arises in the magnetosheath. Our method has the possibility to be extended to three-dimensional, non-axisymmetric modeling by the use of magnetopause normal mapping.

Code and data availability. No codes or data are used in this work.

https://doi.org/10.5194/angeo-2023-2
Preprint. Discussion started: 24 January 2023

Annales Geophysicae Discussions
Open Access
EGU

Author contributions. YN, ST, and DS developed the idea of potential mapping method, checked mathematics, and wrote the manuscript. YN prepared the figures. All authors listed have made a substantial, direct, and intellectual contribution to the work and approved it for publication.

Competing interests. Conflict of Interest: The authors declare that the research was conducted in the absence of any commercial or financial relationships that could be construed as a potential conflict of interest.

https://doi.org/10.5194/angeo-2023-2
Preprint. Discussion started: 24 January 2023

Annales Geophysicae Discussions

References

Angelopoulos, V. The THEMIS mission, Space Sci. Rev, 141, 5, 2008. https://doi.org/10.1007/s11214-008-9336-1

Burch, J. L., Moore, T. E., Torbert, R. B., and Giles, B. L., Magnetospheric Multiscale overview and science objectives, Space Sci. Rev., 199, 5–21, 2016. https://doi/org/10.1007/s11214-015-0164-9

Cairns, I. H., Fairfield, D. H., Anderson, R. R., Carlton, V. E. H., Paularenas, K. I., and Lazarus, A.: Unusual locations of Earth's bow shock on September 24-25, 1987: Mach number effects, J. Geophys. Res., 100, 47–62, 1995. https://doi.org/10.1029/94JA01978

Chakravarthy, S., and Anderson, D.: Numerical conformal mapping, Math. Comp. 33, 953–969, 1979.

Escoubet, C. P., Fehringer, M., and Goldstein, M.: Introduction: The Cluster mission, Ann. Geophys., 19, 1197–1200, 2001. https://doi.org/10.5194/angeo-19-1197-2001

Farris, M. H., Petrinec, S. M., and Russell, C. T.: The thickness of the magnetosheath – Constraints on the polytropic index, Geophys. Res. Lett., 18, 1821–1824, 1991. https://doi.org/10.1029/91GL02090

Fornberg, B.: A numerical method for conformal mappings, SIAM J. Sci. Stat. Comput. 1, 386–400, 1980. https://doi.org/10.1137/0901027

Génot, V., Broussillou, L., Budnik, E., Hellinger, P., Trávníček, P. M., Lucek, E., and Dandouras, I.: Timing mirror structures observed by Cluster with a magnetosheath flow model, Ann. Geophys., 29, 1849–1860, 2011. https://doi.org/10.5194/angeo-29-1849-2011

Guicking, L., Glassmeier, K.-H., Auster, H.-U., Narita, Y., and Kleindienst, G.: Low-frequency magnetic field fluctuations in Earth's plasma environment observed by THEMIS, Ann. Geophys., 30, 1271–1283, 2012. https://doi.org/10.5194/angeo-30-1271-2012

Karageorghis, A., Stylianopoulos, N. S., and Zachariades, H. A.: A numerical conformal mapping method for harmonic mixed boundary value problems, J. Sci. Comp., 11, 167–178, 1996. https://doi.org/10.1007/BF02088814

Kobel, E., and Flückiger, E. O.: A model of the steady state magnetic field in the magnetosheath, J. Geophys. Res., 99, 23617–23622, 1994. https://doi.org/10.1029/94JA01778

Narita, Y., Toepfer, S., and Schmid, D.: Magnetopause as conformal mapping, Ann. Geophys., 41, 87–91, 2023. https://doi.org/10.5194/angeo-41-87-2023

Papamichael, N., and Whiteman, J. R.: A numerical conformal transformation method for harmonic mixed boundary value problems in polygonal domains, J. Applied Math., 24, 304–316, 1973. https://doi.org/10.1007/BF01595198

Schmid, D., Narita, Y., Plaschke, F., Volwerk, M., Nakamura, R., and Baumjohann, W.: Magnetosheath plasma flow model around Mercury, Ann. Geophys., 39, 563–570, 2021. https://doi.org/10.5194/angeo-39-563-2021

Shue, J.-H., Chao, J. K., Fu, H. C., Russell, C. T., Song, P., Khurana, K. K., and Singer,H. J.: A new functional form to study the solar wind control of the magnetopause size and shape, J. Geophys. Res. Space, 102, 9497–9511, 1997. https://doi.org/10.1029/97JA00196

Soucek, J., and Escoubet, C. P.: Predictive model of magnetosheath plasma flow and its validation against Cluster and THEMIS data, Ann. Geophys., 30, 973–982, 2012. https://doi.org/angeo-30-973-2012

Stone, E. C., Frandsen, A. M., Mewaldt, R. A., Christian, E. R., Margolies, D., Ormes, J. F., and Snow, F. The Advanced Composition Explorer, Space Sci. Rev., 86, 1–22, 1998. https://doi.org/10.1023/A:1005082526237

Taŕallyay, M. and Erdős, G.: The evolution of mirror mode fluctuations in the terrestrial magnetosheath, Planet. Space Sci., 50, 593–599, 2002. https://doi.org/10.1016/S0032-0633(02)00038-7

Toepfer, S., Narita, Y., and Schmid, D.: Reconstruction of the interplanetary magnetic field from the magnetosheath data: A steady-state approach, Front. Physics, 10, 1050859 https://doi.org/10.3389/fphy.2022.1050859

Wei, L. K., Murid, A. H. M., and Hoe, Y. S.: Conformal mapping and periodic cubic spline interpolation, Mathematika, 30, 8–20, 2014.